The Pennsylvania State University

DE-FG07-04ID14613

(DOE-NEER Project)

Report for Phase III and final project report

Phase Stability under Irradiation of Precipitates and Solid Solutions in Model Alloys and in ODS Alloys Relevant for GenIV

P.I.: Arthur T. Motta, The Pennsylvania State University,
in collaboration with Robert C. Birtcher at Argonne National Laboratory.

Report Period: Final Project Report (2004-2007)

1. Summary

The overall objective of this program is to investigate the irradiation-altered phase stability of oxide precipitates in ODS steels and of model alloy solid solutions of associated systems. This information can be used to determine whether the favorable mechanical properties of these steels are maintained under irradiation, thus addressing one of the main materials research issues for this class of steels as identified by the GenIV working groups. The research program will also create fundamental understanding of the irradiation precipitation/dissolution problem by studying a "model" system in which the variables can be controlled and their effects understood individually.

In the course of the project, representative samples of several ODS (oxide-dispersion strengthened) steels obtained from three different sources (Pacific Northwest Laboratory, CEA-Saclay and Japan Nuclear Corporation) were characterized using synchrotron radiation diffraction and transmission electron microscopy (TEM) to identify which phases were present and to characterize microstructure. During the third year, a model was developed to predict the evolution of microstructure in the thin films under irradiation, as part of the Ph.D. thesis of Djamel Kaoumi at Penn State.

During the third year of the project, TEM samples were processed from the ODS steels (for microstructure characterization and for the irradiations in the IVEM) by electropolishing method, which proved successful. Fe ion irradiations were carried in the IVEM at 25˚C and 500˚C to high doses. Various effects of ion irradiation were observed as they occurred, including amorphization of large particles, dislocation loop formation, voids, precipitate dissolution and formation.

This report presents a summary of the overall research effort, starting with the characterization of the ODS steels, the irradiation experiments and overall conclusions.

2. Materials Selection and Characterization

2.1 Materials Sources

Various alloys were selected for study among the many ODS steels available. Materials were obtained from three different suppliers: David Gelles at Pacific Northwest Laboratories, (PNNL) , Shigeru Ukai from JNC, and Yann de Carlan from CEA-Saclay. The materials included two heats of MA-957, MA956, the French alloy DY, and the Japanese alloy M16 ODS steel. These alloys have a range of composition and heat treatment and a corresponding range of second phases present.

Because of the nanometer size oxide particles, classical TEM is limited for these materials and the few studies which have been done so far have used HRTEM (for grain size distributions and EDS for composition) but the crystalline structure and lattice parameters of the phases involved still require determination [1-3]. Studies however agree on the fact that the dissolved Y_2O_3 particles reform as clusters of Ti-Y-O compounds which need to be identified. Detailed information about the crystal structure (lattice parameters etc), oxide/matrix interfacial coherency and the formation mechanism of complex oxide particles has not been demonstrated. Such information is needed for controlling physical phenomena in a nanoscale regime, for improving the creep properties at elevated temperature, and also for designing high-temperature structural materials. Synchrotron radiation diffraction can help find more information on the oxide dispersoids.

The materials studied and their compositions are given in Table 1.

Table 1: Compositions of oxide dispersion strengthened (ODS) materials to be studied

Material	Nominal Composition (wt%)	Origin
M16	Fe-9Cr-2W-0.22Ti-0.13C-0.35 Y_2O_3	JNC
	(actual:Fe-8.9Cr-1.95W-0.23Ti-0.14C-0.36 Y_2O_3)	
DY	Fe-13Cr-1.5Mo-1TiO_2-0.5Y_2O_3	CEA-Saclay
MA956	Fe-20Cr-4Al-0.5Ti-0.5Y_2O_3	PNNL
MA957	Fe - 14Cr - 1Ti – 0.3Mo – 0.25Y_2O_3	CEA-Saclay and PNNL

2.2. Materials Characterization

The materials acquired have been studied using synchrotron radiation diffraction in reflection geometry. The samples were examined in theta-two theta geometry, in the two-theta range 5-40 degrees and in the energy range 15-17 keV so that most of the expected second phase peaks and

matrix peaks would be accessible. Synchrotron radiation diffraction can detect small amounts of second phases because of the very large number of photons incident on the sample, combined with very low background.

MA957 ODS steel

The MA957 ODS alloy is a ferritic stainless steel developed by Nickel Company especially for structural reactor applications such as Liquid Fast Metal cooled Breeder Reactors. The alloy as described in its patent (1978) has a nominal composition of Fe - 14Cr - 1Ti – 0.3Mo – 0.25Y_2O_3 (wt%). More generally, the claimed invention is a wrought dispersion-strengthened, heat resistant ferritic alloy having a composition consisting essentially of about 13% to 25% chromium, about 0.2% to less than 2% titanium, up to about 2% molybdenum, up to 2% aluminum, a small but effective amount for improved strength up to about 1.5% yttria and iron for the balance, except for incidental elements and impurities. The alloy can tolerate up to about 4% of nickel, and up to about 2% of manganese and 2% of cobalt and a carbon content up to 0.2% but preferably less than about 0.1%.

The chromium is added to give the alloy oxidation resistance and strength. It also stabilizes the ferritic structure of the steel at elevated temperatures. Alloys having a chromium content less than 13% tend to form austenite upon heating at temperatures higher than 850°C and those having a content of chromium higher than 25% loose ductility. The MA957 alloy contains a nominal 14% of chromium.

Titanium and molybdenum are added in small quantities to improve the ductility and the oxidation resistance of the material. They give solid solution strengthening in iron. Also, they are believed to trap the carbon and nitrogen present in the matrix thus preventing the formation of chromium carbides and nitrides which are a cause for grain boundary embrittlement. Titanium is also believed to prevent chromium volatilization and its concurrent formation of porosity when annealing the alloy at high temperatures. Molybdenum is not an essential component but because it improves the ductility and high temperature strength and the increases room temperature fabricability, it is preferably present in the alloy.

Yttria is added to the material after cold and hot working. The ambient and elevated temperature strength of an alloy can be improved by plastic deformation a.k.a. hot or cold working. However in conventional alloys which do not contain a fine dispersion of a second phase, the strengthening provided by the cold and hot working quickly anneals out when exposed to high temperatures, due to the migration of dislocations and the recrystallization of new grains. The presence of a uniformly distributed dispersoid can prevent recrystallization by blocking the dislocation migration. The advantage of using yttria instead of other oxides, carbides, or nitrides is its relative stability at high temperatures. Other refractory oxides, carbides and nitrides would be suitable as dispersoid materials provided they have such high temperature stability; such suitable dispersoids are thoria, ceria, and rare earth oxides, carbides or nitrides of zirconium, titanium, and hafnium. In addition to high temperature stability it is important to understand stability to irradiation exposure. It is the object of this study. The less desirable materials are alumina, titania, and chromium carbides since it is expected that their size should increase at high temperatures making them less efficient at retarding the recrystallization process. In case

precipitation hardening is relied upon for strength, and the role of the dispersoid as an agent to retard recrystallization is not crucial then titanium precipitation-hardenable phase may actually be suitable.

The alloy is called MA957: “MA” refers to the Mechanically Alloying method employed to process the alloy; and “957” to follow MA956 which is a similar alloy previously processed with chromium content higher than 20 wt%. High energy ball mills and attritors mechanically redistribute the different alloying powder particles on a microscopic scale. The mechanically alloyed powders are then consolidated by hot extrusion in an evacuated steel can. The resulting wrought bar is hot-worked and then cold-worked into its final geometry prior to fabrication into a finished product and sale.

The piece of MA957 ODS steel provided by CEA at Saclay is shown in figure 1 . Two types of samples (transverse and circumferential) were processed from the original piece in two different orientations.

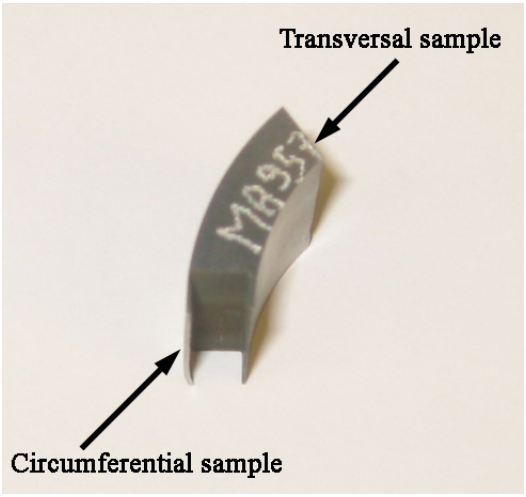

Figure 1: Piece of MA957ODS Steel from CEA Saclay, showing two different orientations.

Synchrotron radiation X-ray Diffraction: Figures 2 and 3 show the XRD spectra obtained for MA957 (from CEA) from the theta-2theta run in the synchrotron from the circumferential sample. Both orientations (transverse (figure 2) and circumferential (figure 3)) were examined, and in both cases the phases shown were bcc-Fe (peaks indexed in black and $Y_2(C,O)$ (peaks indexed in color). This last phase is cubic, with a =0.424 nm (PDF#22-0959). The peaks associated with the dispersion are very broad and may include 2 or more convoluted peaks. The crystallographic structure of the Y_2O_3 powders initially introduced does not show. They seem to have undergone dissolution/reprecipitation during the mechanical-alloying/heat-treatment fabricating process. As for the Fe matrix, the (110), (200), (211) peaks show similar intensities in contrast with the transversal sample where the (110) peak is more pronounced, revealing a preferred orientation of the grains. This can be related to the lamellar structure that the TEM micrographs of the transverse samples as shown in Figure 4.

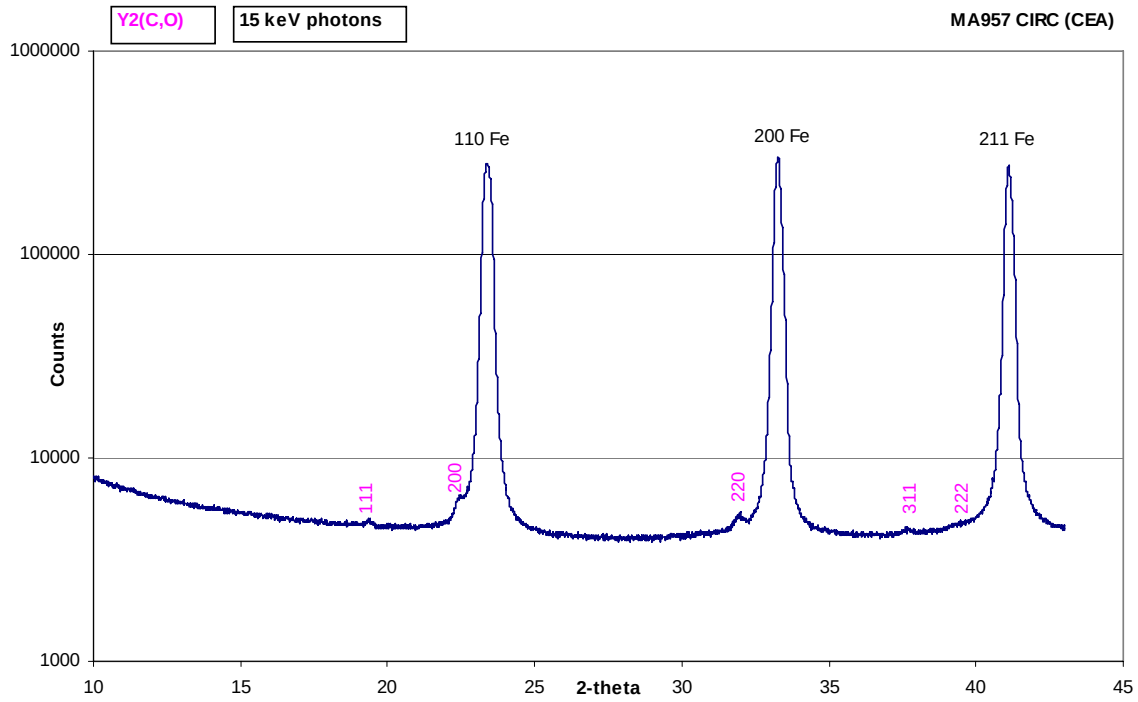

Figure 2: X-ray diffraction intensity versus two theta angle obtained using 15 keV synchrotron radiation the circumferential orientations of CEA MA957.

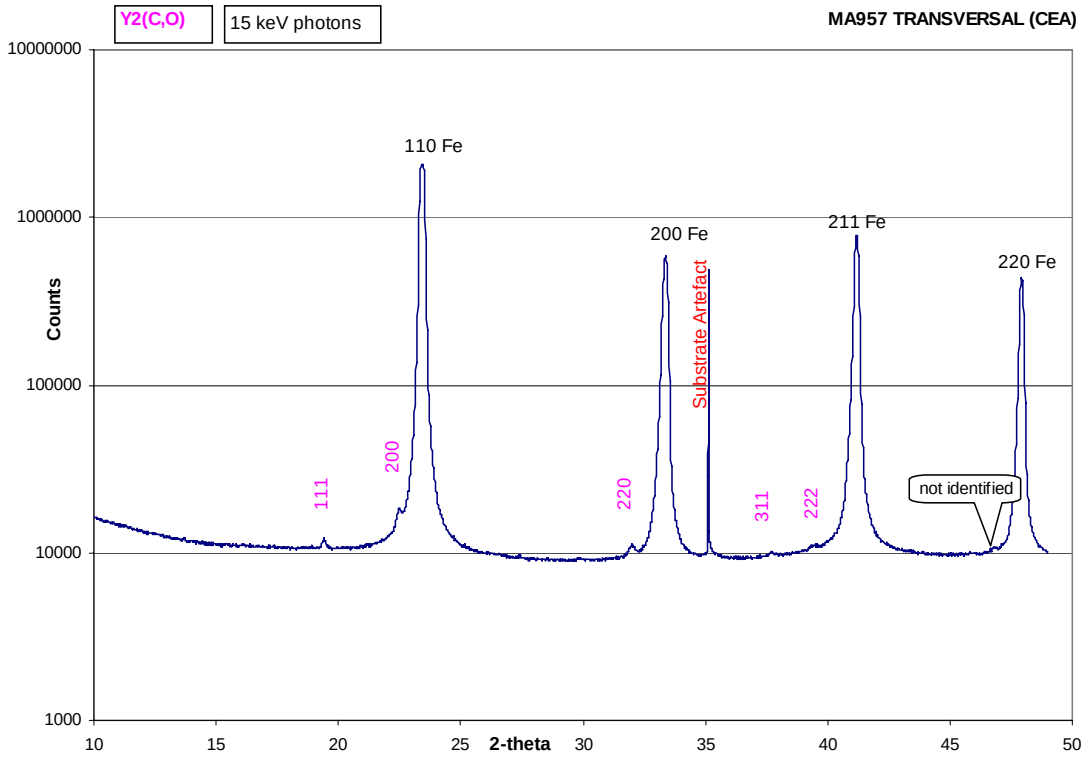

Figure 3: X-ray diffraction intensity versus two theta angle obtained using 15 keV synchrotron radiation from transverse orientation of MA957.

TEM analysis: Both types of samples (transverse and circumferential) were prepared by electropolishing. These are both shown in the composite figure 4. In the circumferential orientation, the grains are more or less isotropic. Some grains show a high dislocation density while others do not as can be seen on Figure 4. The oxide population shows a wide range of sizes from a few nms to hundred of nms. In the transverse direction, the TEM micrographs of the transversal cut of the MA957 piece show a lamellar structure. Overall, the alloy is very compact with no pores visible. From this point of view it is comparable to the steels produced by melting.

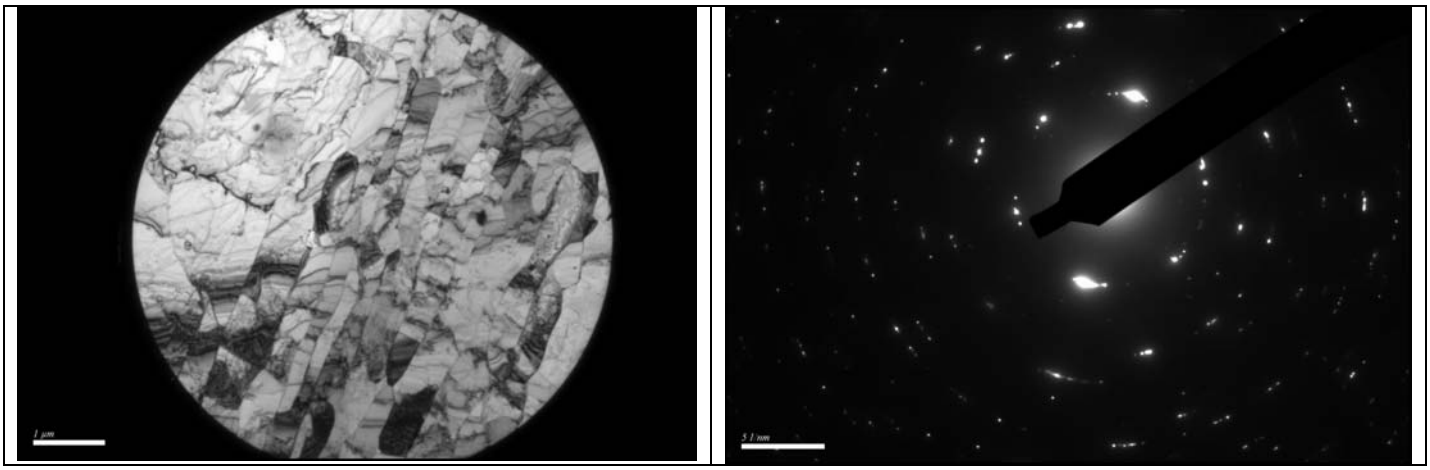

Figure 5: Bright field image showing selected area in MA957 transverse sample and corresponding diffraction pattern, from bcc Fe, showing the texture of the material (preferential orientation of the grains).

Figure 5 shows a bright field image and diffraction pattern from this alloy. The diffraction spots are aligned with the rolling texture.

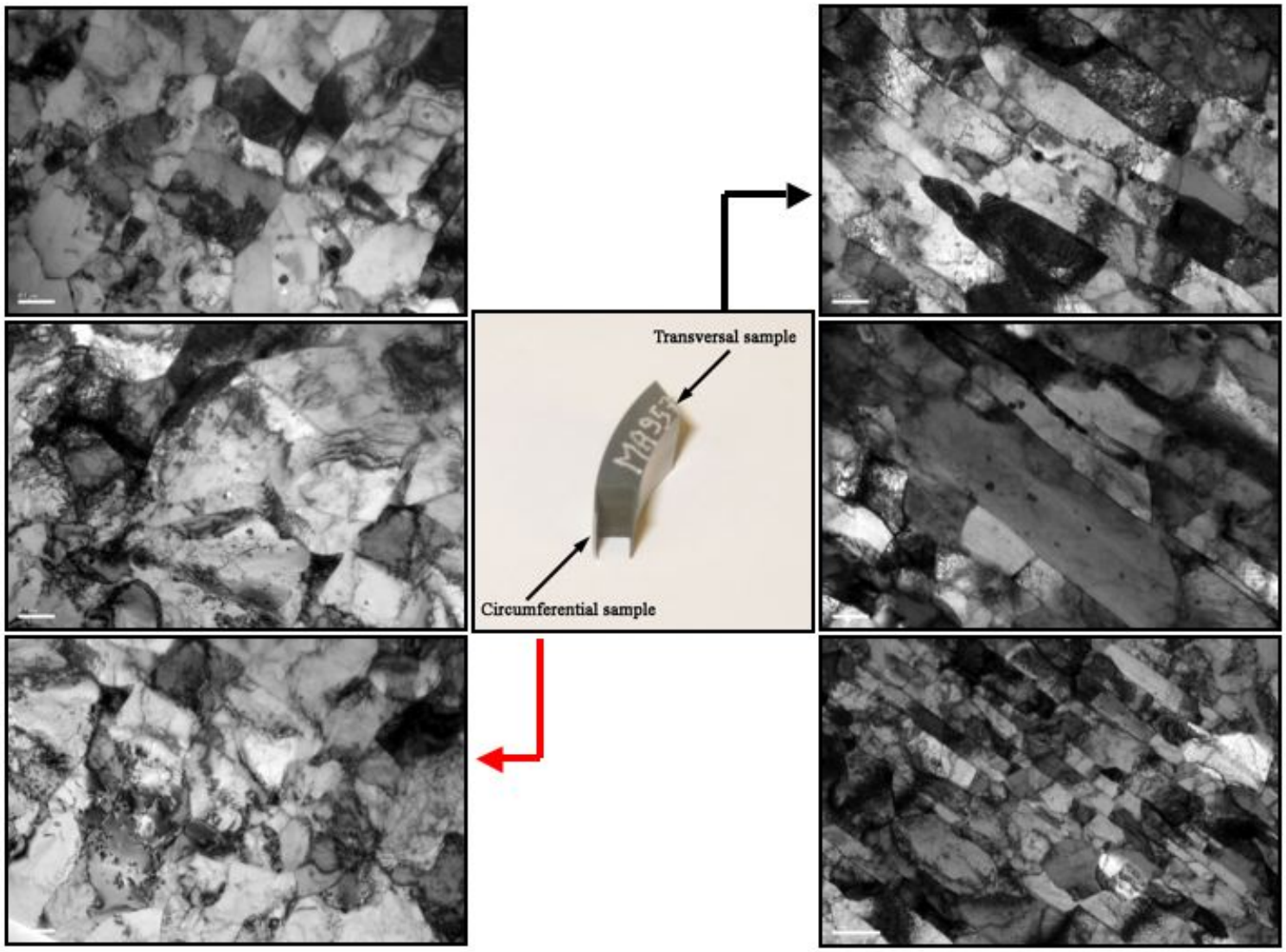

Figure 4: Bright Field TEM images of the grain microstructure in MA957 ODS steel in the circumferential and transverse direction

DY alloy

The alloy named DY is a ferritic ODS steel developed by CEN-SCK Mol (Belgium) and fabricated by Dour Metal by mechanical-alloying of metal powders with Y_2O_3 and TiO_2 powders. The alloy nominal chemical composition is Fe –13Cr –1.5Mo –1TiO_2–0.5Y_2O_3 (wt%). After the powders are mechanically alloyed in a vibrating ball-mill, they are cold-pressed, and then hot-isostatic-pressed at 950°C. The extrusion in form of tubes is done at 1150°C with a glass lubricant. The intermediary thermo-mechanical treatment is proprietary. The DY material was provided by the CEA (Saclay, France) as a tube with 6.55 mm outer diameter and 5.65 inner diameter. This is an example of the first generation of ODS steels designed in the 1980s.

X-Ray Synchrotron radiation Diffraction:

a. X-ray analysis:

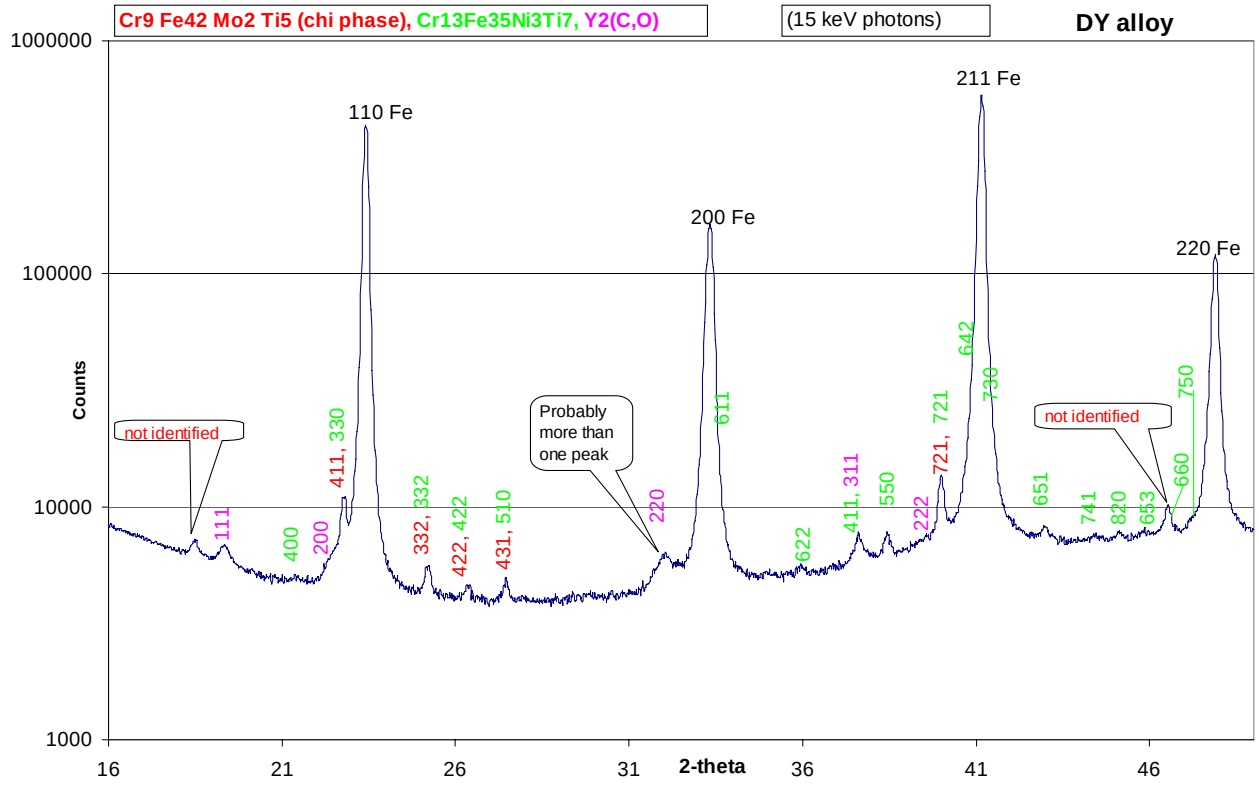

Figure 6: X-ray diffraction pattern obtained from synchrotron irradiations of alloy DY:

The oxides initially introduced were TiO_2 and Y_2O_3 (lanthanide sesquioxyide structure; cubic centered; a=1,0604 nm). The X-ray diffraction spectrum (figure 6) clearly shows that after the processing of the alloy (mechanical milling and thermo-mechanical treatment) the oxides have changed composition and structure, since none of the peaks corresponding to the initial oxide structure are apparent The initial oxides have most likely dissolved during the mechanical alloying process and re-precipitated during the thermo-mechanical treatment. A set of

unidentified peaks is noted in the spectrum. They are most likely associated with oxide aggregates.

New intermetallic phases have also formed during the processing of the alloy. The χ phase ($Fe_{42}Cr_9Ti_5Mo_2$) has an ordered structure of the type of α-Mn, with 58 atoms per unit cell and a cell parameter of 0.886 nm. Another intermetallic richer in chromium is also indexed in the XRD spectrum, the formula of which is $Fe_{35}Cr_{13}Ti_7Ni_3$. Ni is not an alloying element initially introduced and may come as an impurity from the milling atrium. The matrix is a soft steel [4] but no information is available on the exact nature (chemical formula).

TEM analysis: The microstructure is composed of two types of grains, with respect to dislocation density. The first type contains few dislocations (recrystallized grains) and the other shows a high tangled dislocation density. When present, many dislocations are anchored in the oxide particles as can be seen in Figure 7.

All grain boundaries are decorated by an intense precipitation of the quaternary intermetallic χ phase ($Fe_{42}Cr_9Ti_5Mo_2$), which is detrimental to the mechanical properties of this alloy (creep). These grain boundary intermetallics are very thick: 0.5 to 1 micron width as can be seen in Figure 8. Homogeneity of the oxide dispersion within the material is a critical feature. In the samples processed for this study, the oxide dispersion appears homogeneous throughout the grains i.e. no difference in oxide distribution has been observed between grains in the circumferential direction (only circumferential samples prepared for DY). The oxide dispersion includes very fine oxides (less than 10 nm) which are not always visible (depending on the matrix orientation) and bigger ones (up to hundreds of nms).

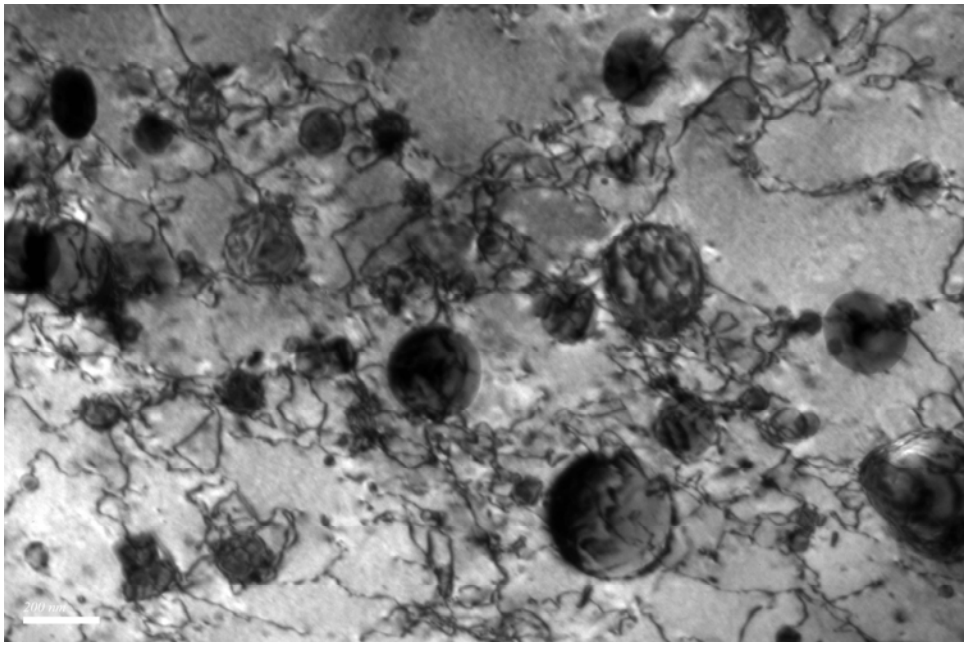

Figure 7: Bright field micrograph of dislocations structure in DY showing interaction of dislocations with the particles: (anchoring of dislocations in particles)

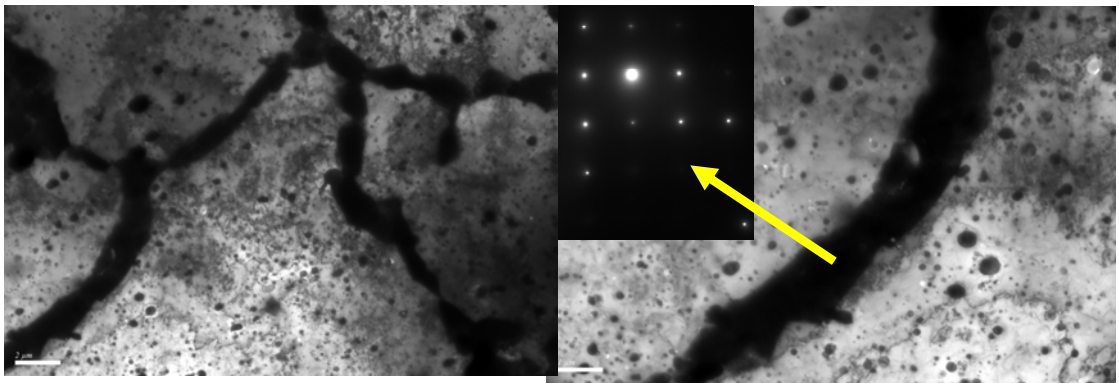

Figure 8: DY microstructure showing grains with low-density dislocations. Grain-boundaries are decorated with the intermetallic χ phase (0.5 to 1 micron thick).

JNC (M16) alloy:

The composition of the ODS steel provided by the Japanese Nuclear Commission is:

Weight %	Fe-9Cr-2W-0.2Ti-0.13C-0.35 Y_2O_3 (wt%)
Atomic %	Fe-9.68Cr-0.61W-0.23Ti-0.61C-0.17Y-0.26O (at%)

Synchrotron radiation X-ray Diffraction analysis: Figure 9 shows the analysis of the JNC alloy. In addition to the bcc phase, many peaks associated with mixed-metal carbides of the form $M_{23}(W,Mo)_2C_{12}$ are indexed, and a few unidentified peaks are arrowed. Once again, the XRD spectrum shows absence of the peaks from the initial oxide structure. The particles have changed chemical composition and structure. The as-received alloy has a dispersion of carbides and oxides. This point highlights once again the critical impact of impurities (such as C) and the thermo-mechanical treatment on the initial dispersoid during the fabrication of the alloy.

Another interesting result of the x-ray diffraction study was that the fitting of the bcc peaks in all the alloys show a superposition of two different peaks, appearing to correspond to two different bcc phases with slightly different lattice parameters which can result for example from grains with different Cr content. This is shown in Figure 10, which shows on top a bcc 110 peak from this alloy. These peaks were fit using PeakFit software and as shown in the bottom they require two separate peaks to be properly fitted. The two peaks correspond to two values of lattice parameter of 0.2884 nm and 0.2874 nm.

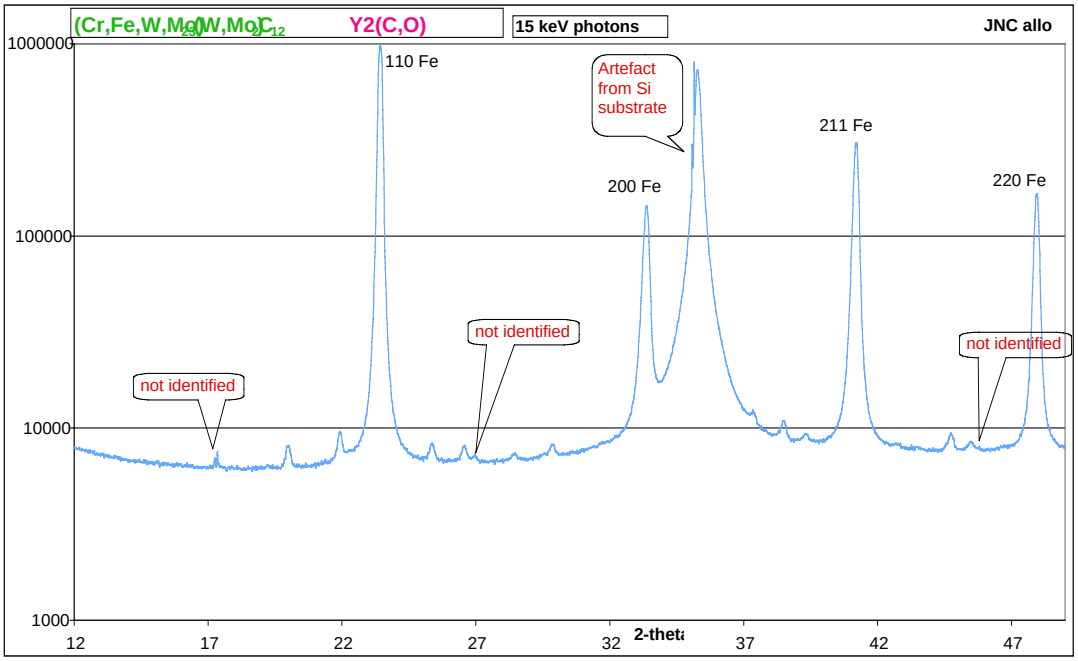

Figure 9: X-ray diffraction pattern from synchrotron irradiation of M16 alloy from JNC. Carbides are formed during the mechanical alloying process; peaks from the initially formed Y_2O_3 phase are not apparent; instead $Y_2(O,C)$ and some unidentified peaks are present.

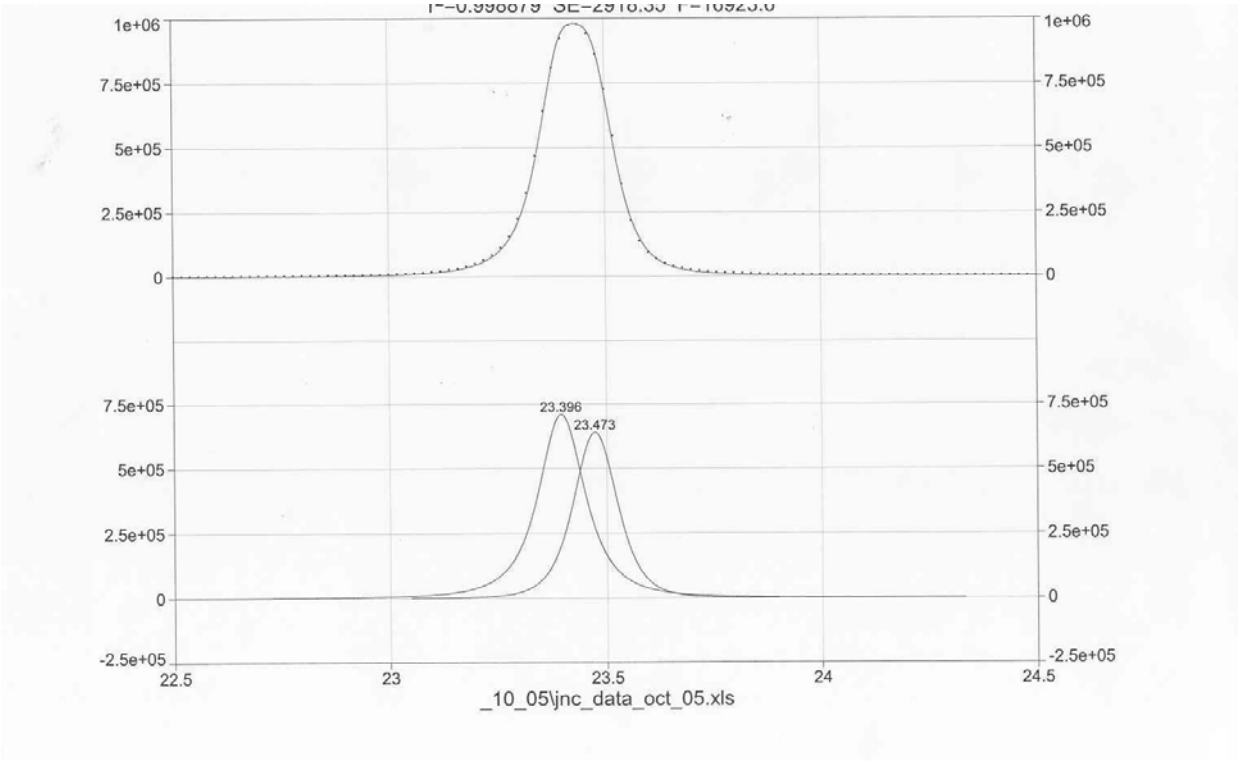

Figure 10: Analysis of bcc 100 peak showing a split in the peak.

TEM analysis:

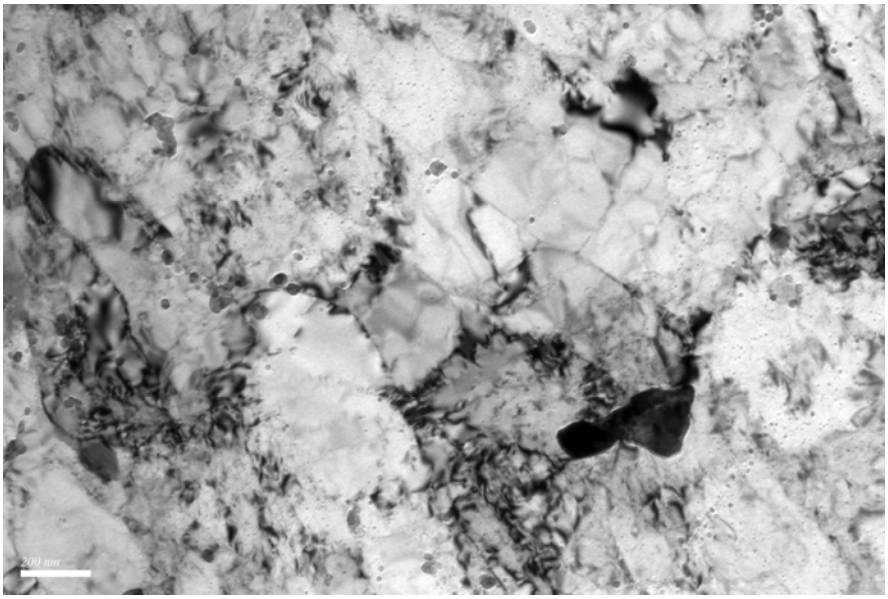

Figure 11: Bright field micrograph of the JNC M16 alloy in the as-received state.

The grain morphology of JNC M16 alloy (figure 11) is not directional as in the case of MA957 CEA which showed pancake shape grains in the direction of extrusion, and the overall grain size is smaller. Random grain orientation is also visible in the diffraction pattern (figure 12).

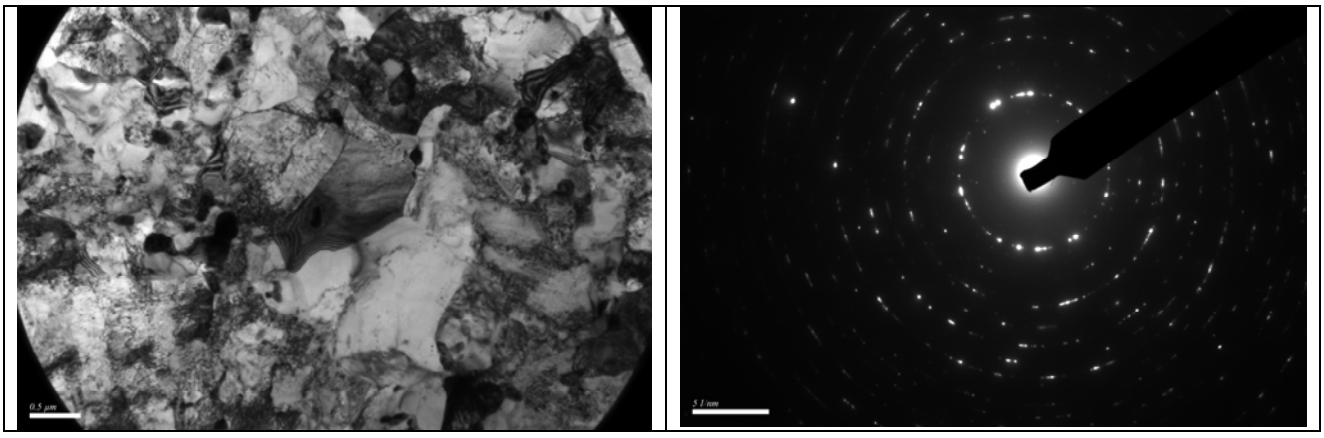

Figure 12: a) Bright Field micrograph; b) corresponding diffraction pattern showing random orientation in the grain population.

There are two populations of precipitates size-wise: relatively coarse ones (a few tens of nanometers up to hundred nms) versus very fine particles (less than 10 nm). Among the small precipitates there are two populations of precipitates with respect to the behavior going through focus: some precipitates go from white contrast to black contrast while the others exhibit the inverse behavior. This is an indication of different electron density within these precipitates, thus possibly different chemical composition. This is to be related with the XRD results showing two

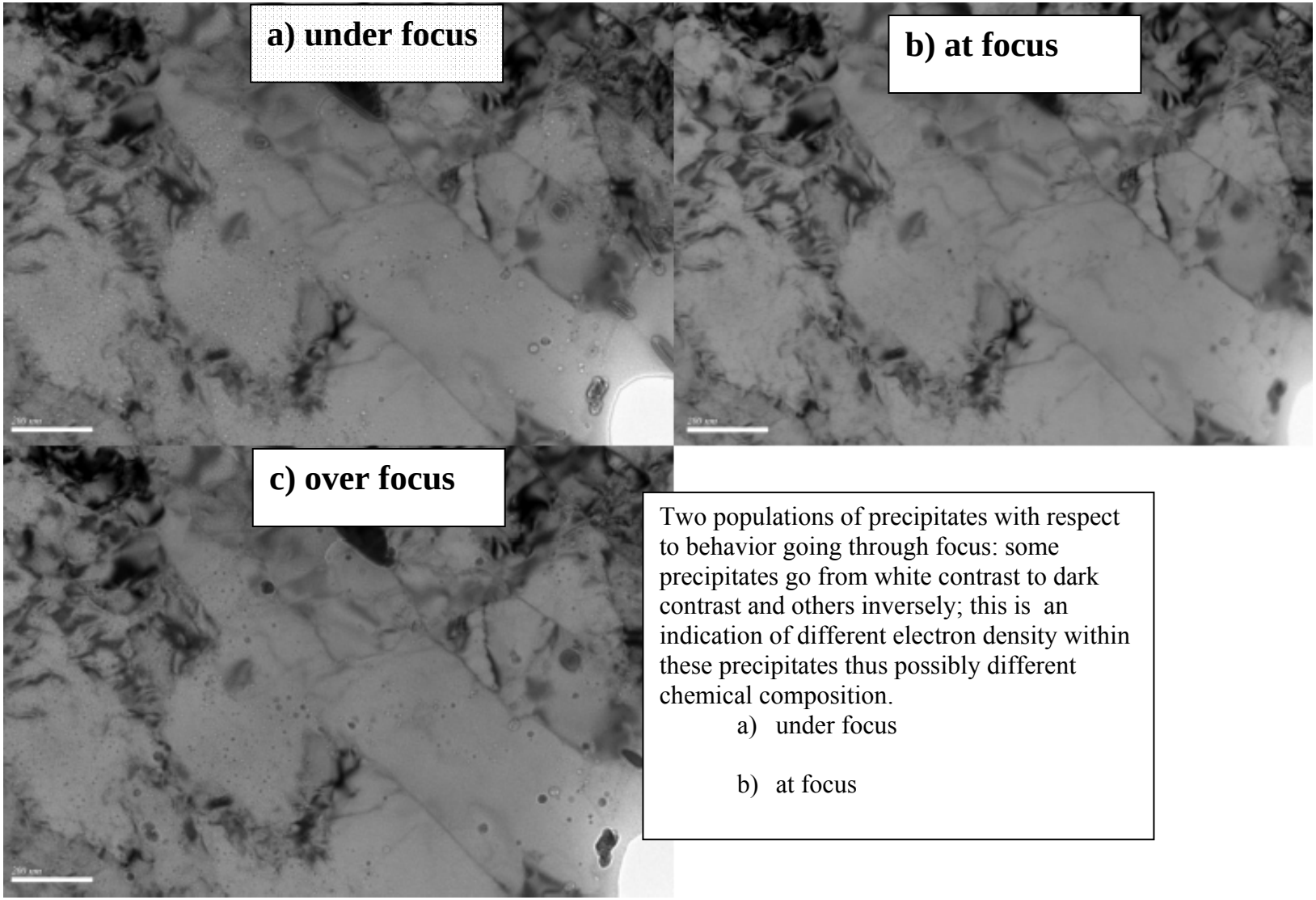

Figure 13: Evidence of two types population of precipitates. (a) underfocus, (b) at focus and (c) overfocus.

types of precipitates (oxides vs. carbides) (Figure 9). TEM diffraction is limited for identifying such small-sized precipitates; for the same reasons, EDS cannot be used to identify the crystal structure of these precipitates; since because the size of the beam is bigger than the precipitates, it includes signal from the matrix. Energy filtering using a GIF on a microscope would be beneficial for chemical analysis in the sample but was not available at the time of study.

MA956 (from PNNL)

Figure 14 shows the diffraction pattern of MA956 sample obtained from PNNL. In addition to the bcc peaks, we observed broad peaks that were tentatively indexed as $YAlO_3$, with a cubic structure (PDF#038-0222). Alamo et al.[1] studied MA956 and MA957 with TEM: two populations of oxides were found: very fine particles (< 50 nm), and bigger dispersoids. X-ray diffraction patterns of the residues obtained after electrochemical dissolution of the ferritic matrix were obtained. The bigger particles were identified as Ti and Al compounds like TiN and Al_2O_3; however the Al compounds were not pure Al oxides, they were usually associated to titanium oxide (TiO_2).Other particles were detected and identified as the Yttrium compounds like $YAlO_3$ (only in MA956) and $Y_2Ti_2O_7$.

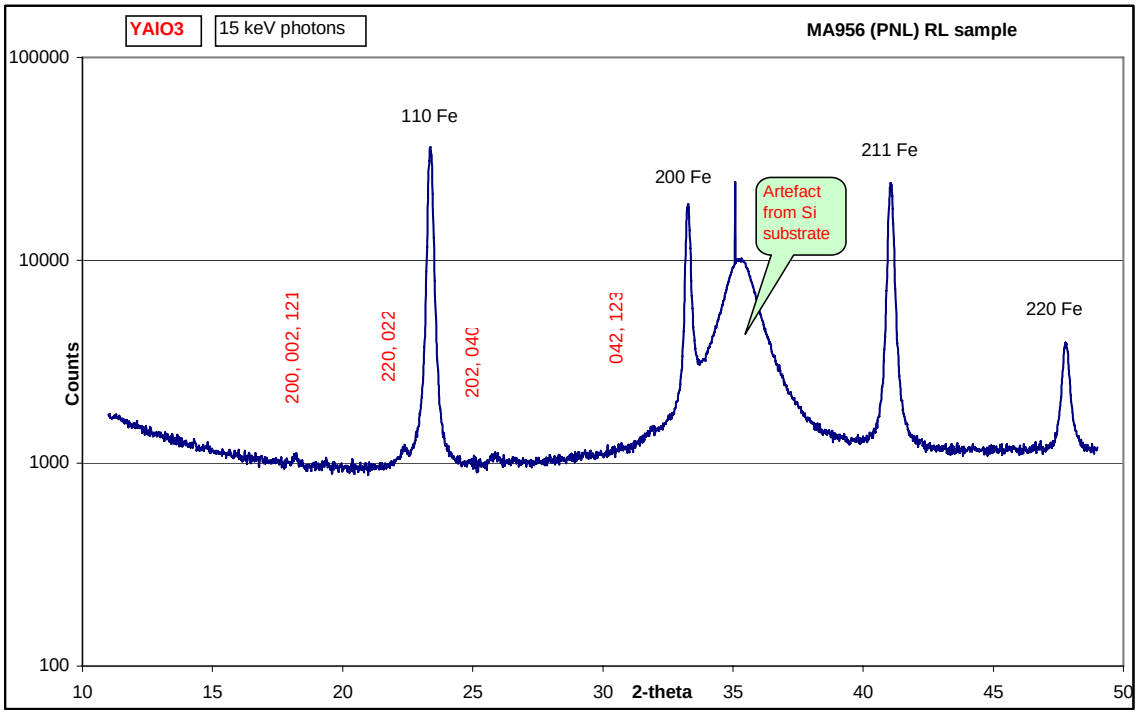

Figure 14: X-ray diffracted intensity versus two theta angle for MA956 alloy from PNL.

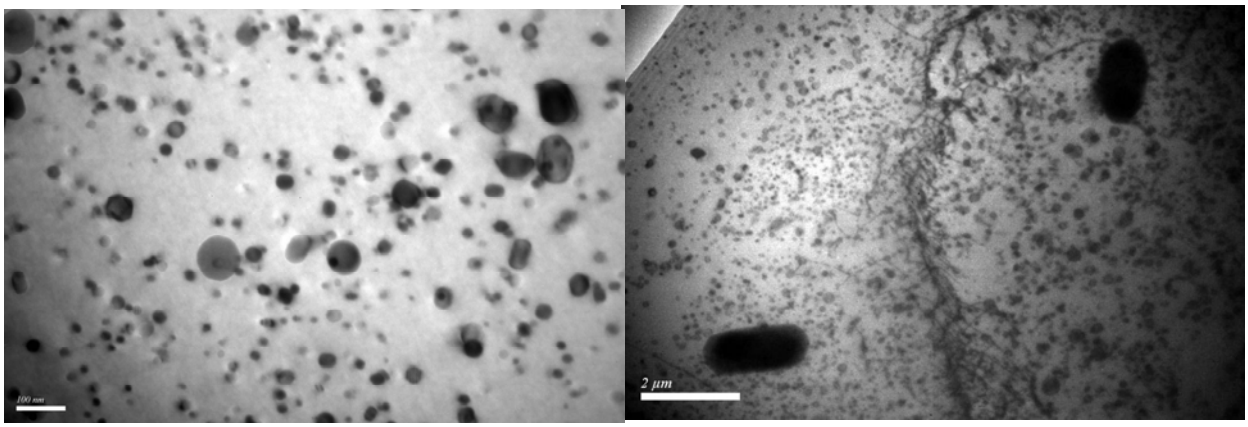

Figure 15: Bright Field micrograph in MA956 showing two precipitate populations.

3. In-Situ Ion irradiation of the ODS steels

The ion irradiations were conducted at the Intermediate Voltage Electron Microscope (IVEM)-TANDEM facility at Argonne National Laboratory, where an ion accelerator is attached to an electron microscope operated at 300 keV [5] so that microstructure evolution can be followed *in situ* on the microscope. Samples were irradiated with 300keV Fe ions, at 300 K and at 773 K. The displacements rate was calculated using the Monte Carlo program SRIM2003[6]. Although higher doses can be reached with noble gas ions rather than metal ions, we have chosen self-ion irradiations to avoid gas ion implantation which can happen with noble gas ion irradiations. Ion fluxes were typically around 2.50×10^{11} ions/cm^2-s.

3.1 300 keV Fe ion irradiation of DY

The DY sample was irradiated in situ in the IVEM at 300 K to 3.5×10^{15} ions/cm^2. Figure 16 shows a bright field of the irradiated microstructure after an intermediate ion dose.

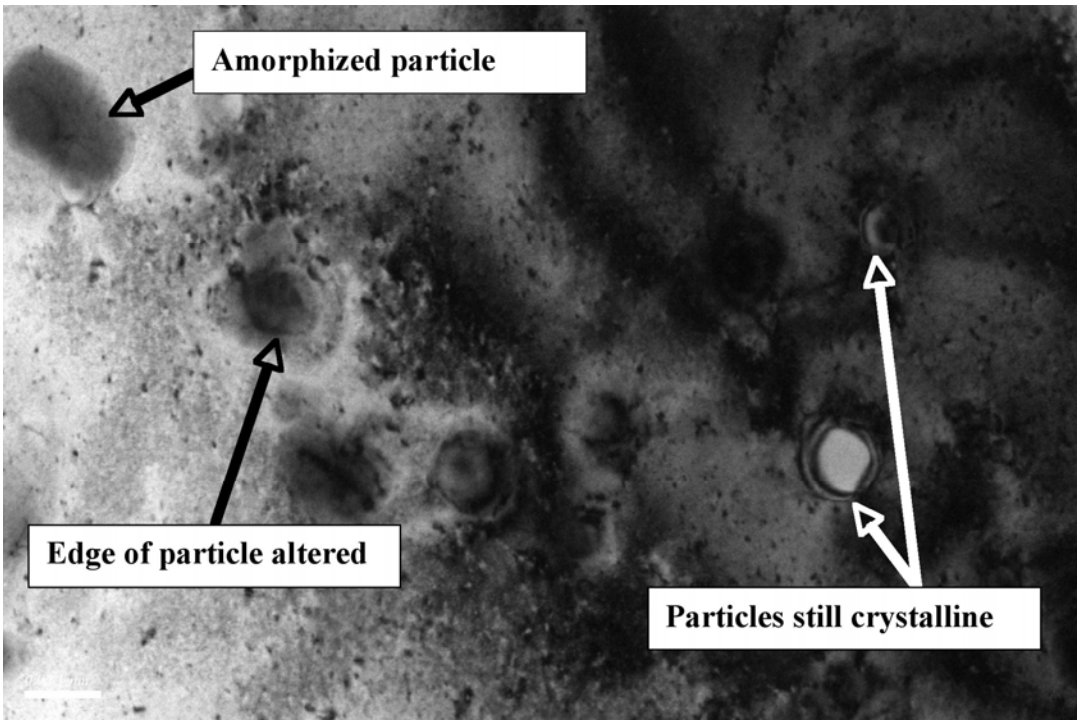

Figure 16: Bright Field micrograph showing effects of 300 keV Fe ion irradiation on DY at 300 K particles are altered rather early: some remain unchanged, others remain crystalline but show an altered interface and others are completely amorphized.

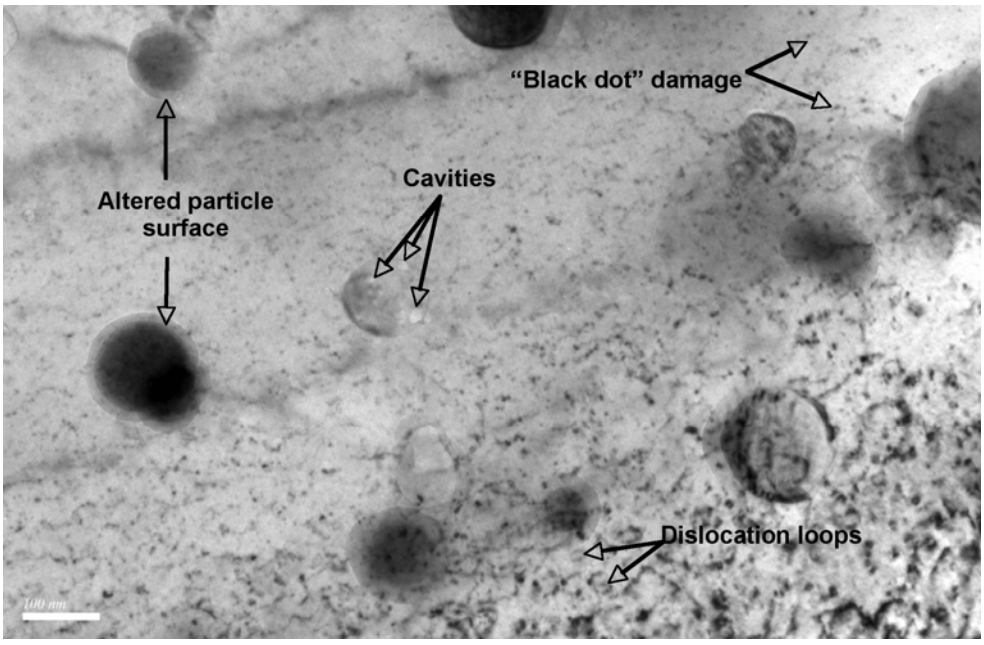

Figure 17: DY irradiated at 300 K with 300 keV Fe ions to ~12 dpa

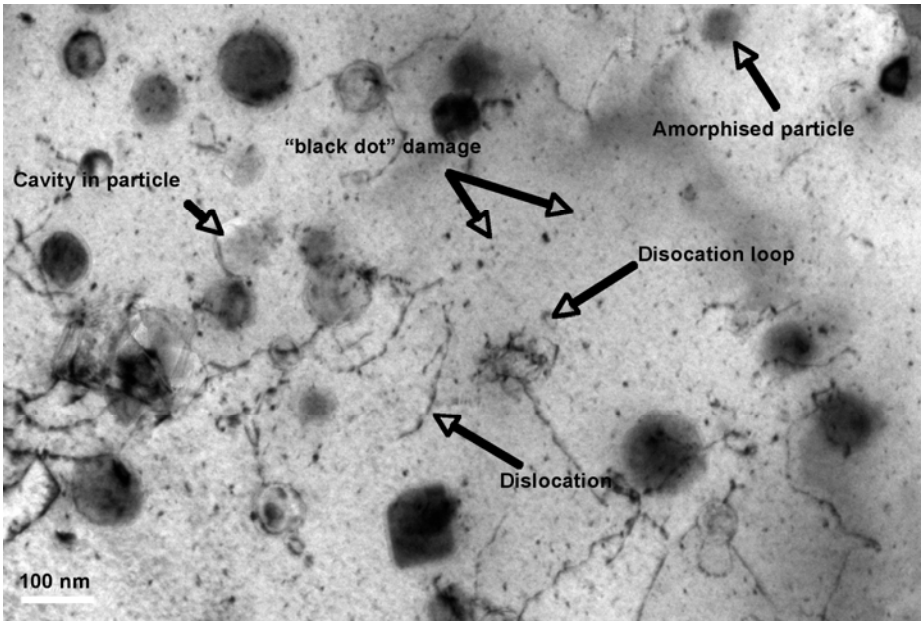

Figure 18: 300 keV Fe ion irradiation at 300 K to ~12 dpa

The Fe ion irradiations of DY at 300 K show that degradation of particle interfaces starts rather early in the irradiation stage as seen in Figure 16. Some of the particles undergo amorphization. while others are resistant to amorphization (and therefore are still crystalline after irradiation,) This difference in behavior may come from the difference in chemical composition. Amorphization was not observed in the neutron irradiations (435 to 580ºC) of the same alloy. This difference may be due to the difference in dose rate between ion and neutron irradiations; Amorphization may be possible with neutrons at lower temperatures since there is usually a shift in temperature range between ion and neutron irradiations due to the difference in dose rate (as is the case for void swelling)[Motta, 1991 #151].

The small size particle population is more difficult to observe because of the irradiation damage (even though the dose in not very high.) During neutron irradiation, it was reported that the small size oxides disappeared at high doses (~200 dpa). Also in the neutron irradiations, the big precipitates which dissolve are surrounded by a "halo" of small precipitates. It was suggested that the phenomenon of re-precipitation may have happened after the irradiation was stopped while the DY tube was still in the reactor cooling down; indeed the alloy stayed in the reactor for about 600 hours and therefore spent an equivalent 600 h at 400ºC. If it is the case, re-precipitation is not expected to occur under ion irradiation even for high temperature irradiations because the cooling rate after the irradiation is complete is very fast and would be equivalent to quenching the material.

Small cavities are observed in the ion irradiation case as shown on figure 17-18 , mainly associated with particles. The density of these voids is not numerous and they are very small; but higher doses need to be reach to derive more definite conclusions. The formation of the same type of small cavities was reported by I. Monnet [4] at 435˚C and 450˚C in the DY under neutron irradiation (54.8 and 62 dpa respectively). At 435˚C, more so than at 450˚C; also, at 435˚C, Monnet reports cavities in the matrix but no cavities at 450˚C.

3.2 300 keV Fe ion irradiation of ODS MA957 TRANS at 25˚C

In this sample, only some oxide precipitates have an altered edge as shown on figures 18 and 19, and yet the XRD spectrum shows only one type of dispersoid: oxides. Why some are dissolved quicker than others may just be because of different local chemical composition. Overall, oxides are more stable with respect to amorphization in this MA957 steel, relatively to DY and JNC. Completely amorphized particles are harder to find in irradiated MA957, whereas amorphization occurred much more readily in DY and JNC sample at the same irradiation temperature. It could be that in the case of DY and JNC the particles which are more sensitive to amorphization are the carbides or intermetallics which are not present in this alloy according to the XRD spectrum.

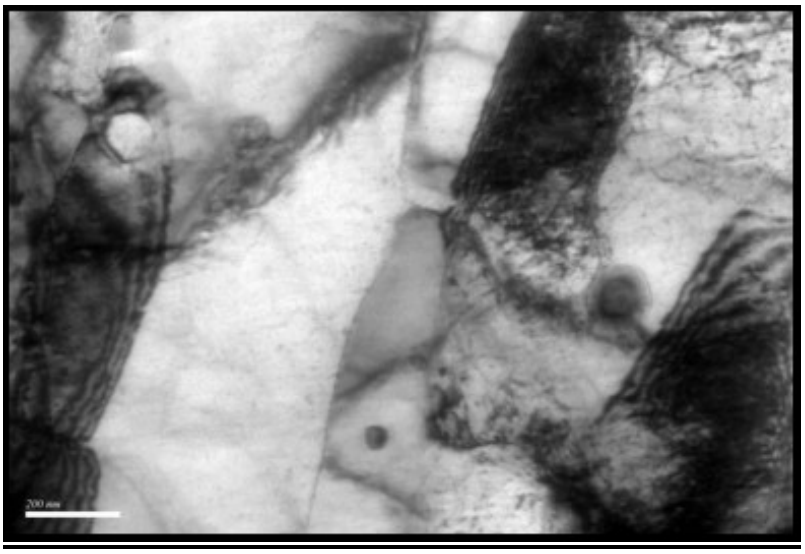

Figure 19: MA957 TRANS irradiated with 300 keV Fe ions at 25˚C to $3x10^{15}$ ions/cm^2

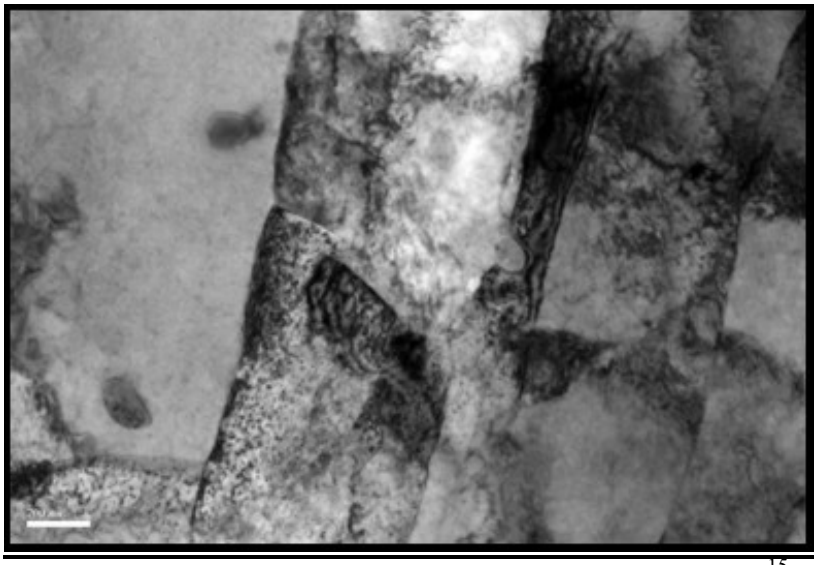

Figure 20: MA957 TRANS irradiated with 300 keV Fe ions at 25˚C to $3x10^{15}$ ions/cm^2 (other area)

300 keV Fe ion irradiation of ODS M16 alloy from JNC

Irradiations at 25˚C:

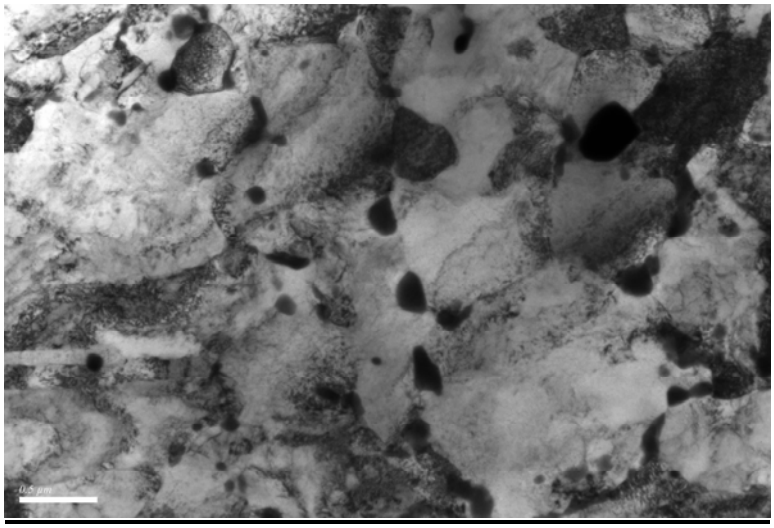

Figure 21: Bright field micrograph of ODS M16 alloy from JNC to a total fluence of $2x10^{15}$ ions/cm^2 : the bigger precipitates are amorphous

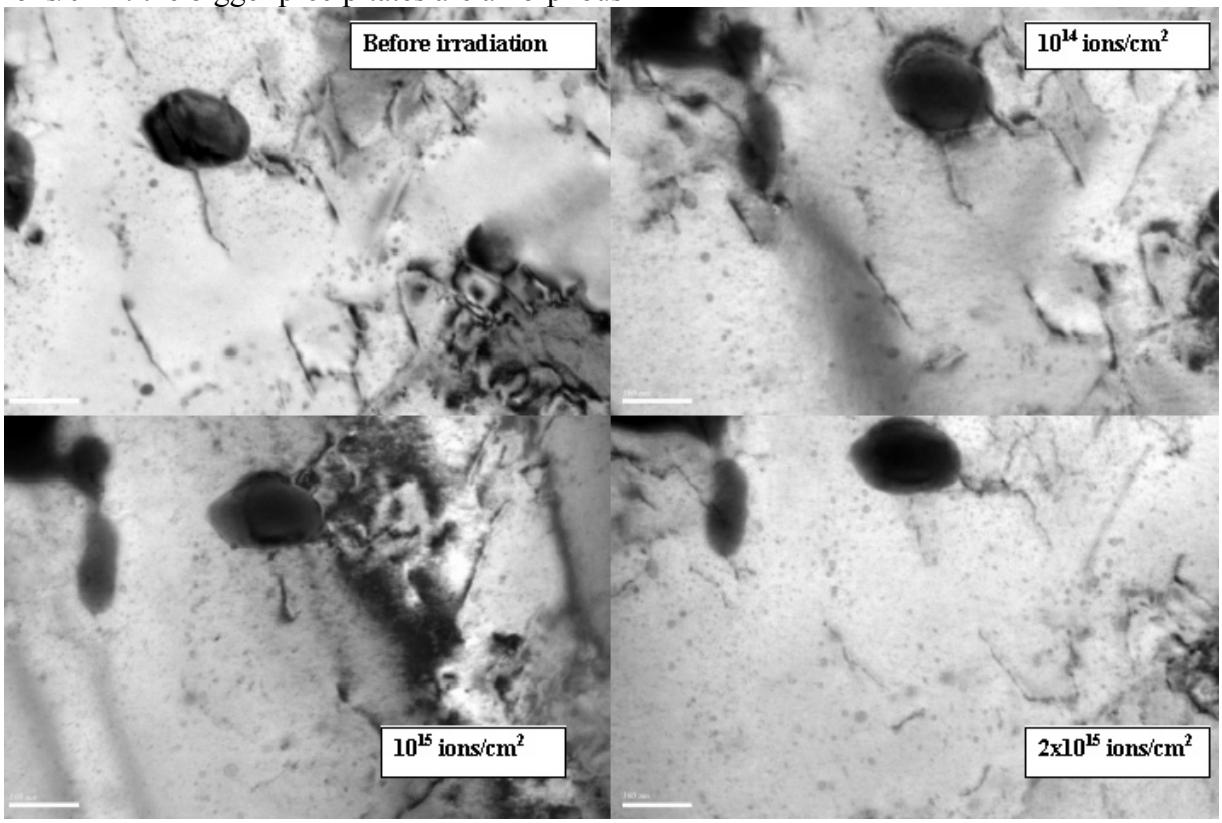

Figure 22: Oxide evolution under 300 keV ion irradiation at 25˚C: the particle is amorphized.

300 keV irradiation at 500˚C

Two regions were followed under irradiation at this temperature, which showed two different features: Figure 23 follows the evolution of a few precipitates under irradiation: as one would expect they appear more stable than at 25˚C with respect to amorphization; however the changes in morphology indicates dissolution at the edges of the precipitate. Figure 25 show another region illustrating how big precipitates serve as nucleation center for second phase precipitation (red arrow). Under irradiation the growth of the nuclei by coalescence is also observed as indicated by the black arrows.

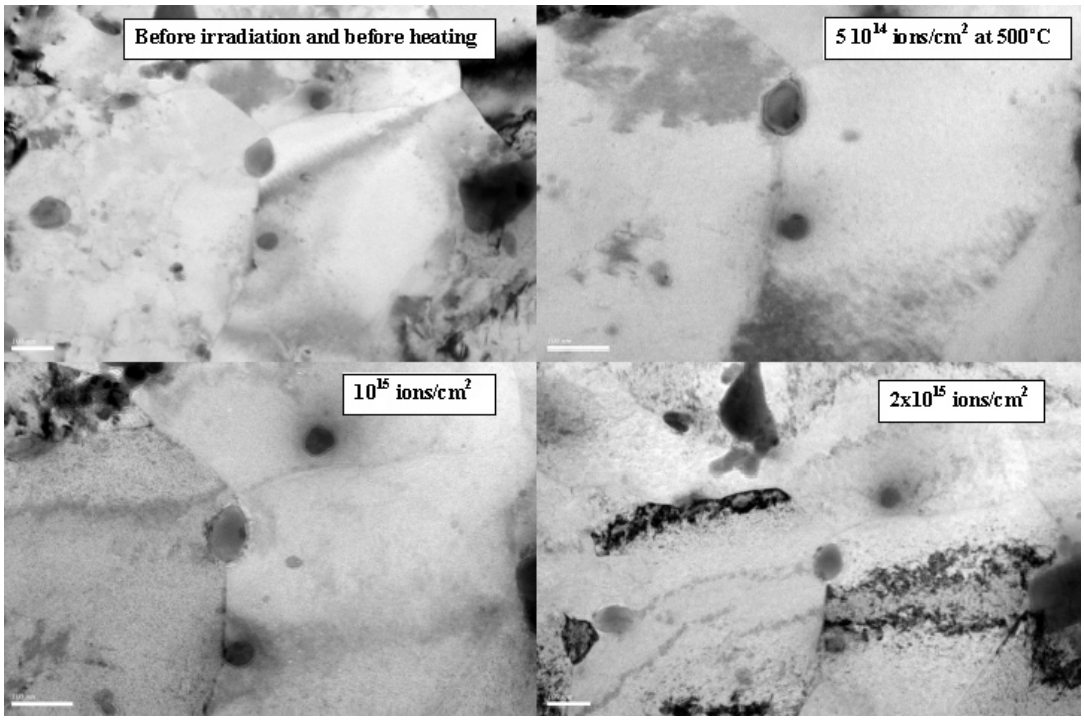

Figure 23: Precipitate evolution under 300 keV Fe ion irradiation: the particles remain crystalline but morphology changes at the edges.

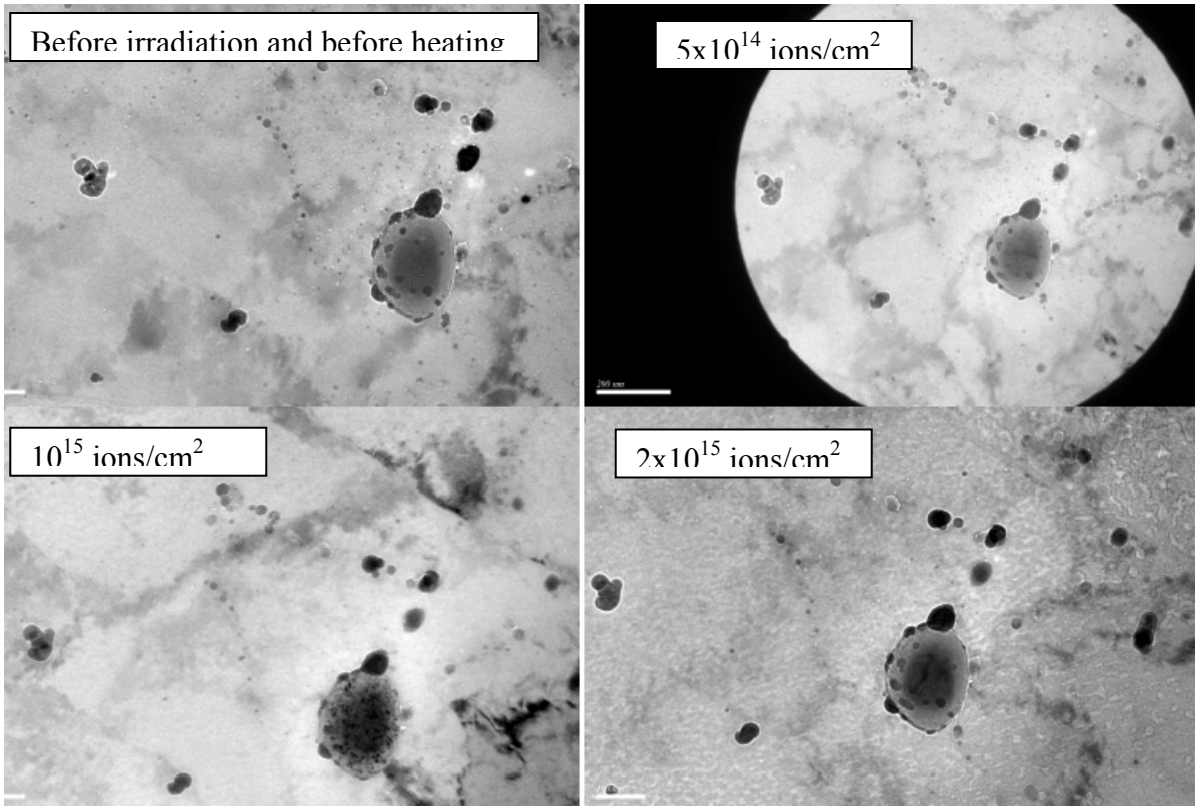

Figure 24: M16 sample irradiated with 300 keV Fe ion at different doses (other region) showing how big precipitates act as nucleation centers for second-phase precipitation (First and last micrographs are taken in slightly under-focused condition for better contrast

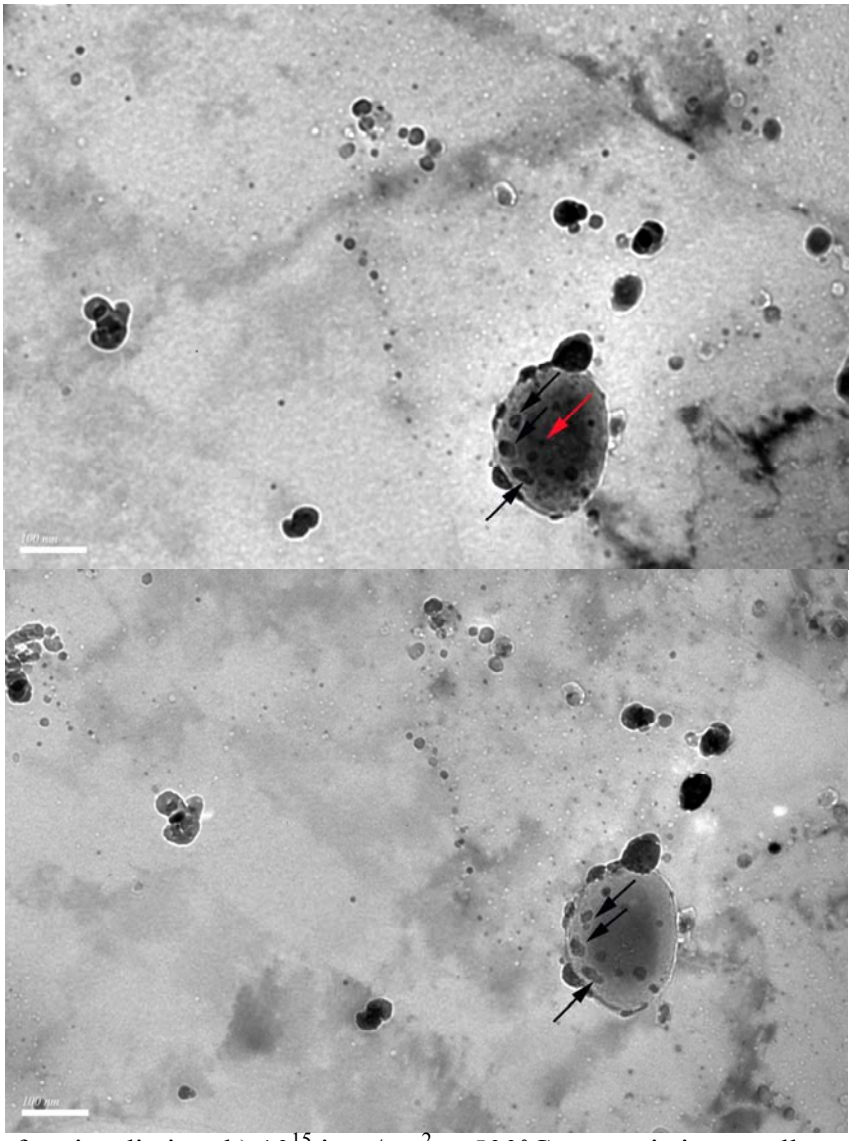

Figure 25: a) before irradiation; b) 10^{15} ions/cm^2 at 500˚C: pre-existing small nuclei have coalesced (black arrows) and new nucleus is formed (red arrow). This highlights the role of big precipitates as a nucleation center for the carbides (micrographs are taken in slightly under-focused conditions for better contrast.

After stopping the irradiation, the sample was left in the TEM at 500˚C for less than one hour. Extensive precipitation throughout the matrix occurs as shown in figure 26. This was not a contamination effect related to the electron beam as the same effect was observed in other areas which were not hit by the electron beam during the experiment; this phase could be α' in this range of temperature.

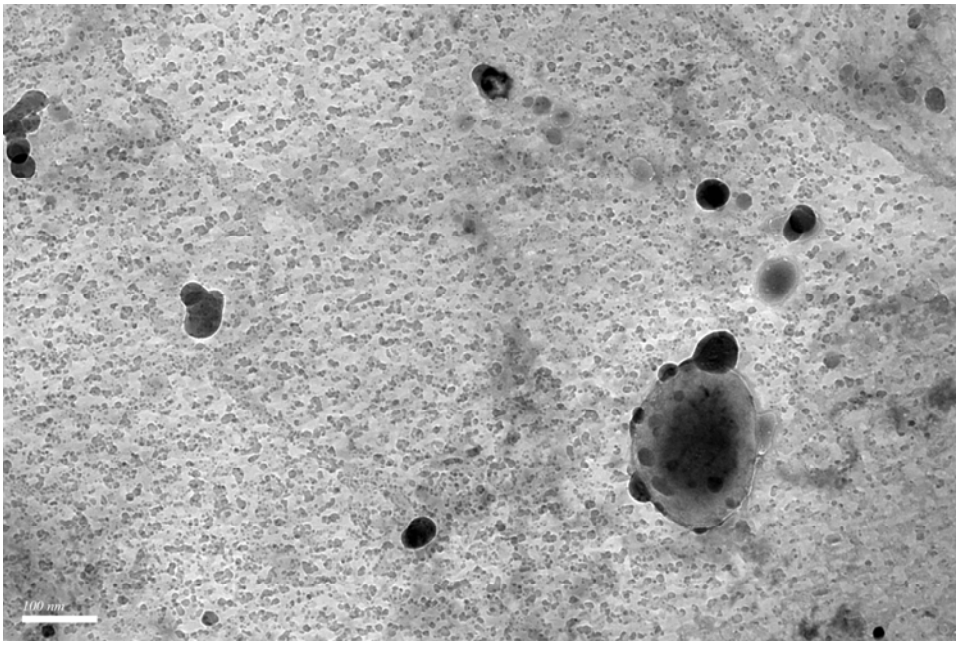

Figure 26: After stopping the irradiation, the sample was left in the TEM at 500˚C for less than one hour. Extensive precipitation throughout the matrix occurs.

SUMMARY:

Prior to irradiation:

- Grain morphology is not directional as was the case of MA957 CEA which showed lamellar-like grain structure in the direction of extrusion.
- 2 populations of precipitates size-wise
- 2 populations of precipitates with respect to behavior going through focus: some precipitates go from white contrast to dark contrast and others inversely; this could be an indication of different electron density within these precipitates thus different chemical composition.

After irradiation at 25˚C:

- Large precipitates become more diffuse or amorphous-like / less responsive to tilt
- Density of line dislocations appears to decrease; DP seems a little "cleaner"
- Morphology changes at the edges of the precipitates
- Small precipitates still present but harder to find.

At higher temperature (500˚C):

- Less irradiation defects visible than at Room Temperature
- At end of irradiation, the sample is left at 500 C for ~one hour: extensive precipitation occurs within the matrix; second-phase precipitates respond all in the same direction when going through focus. This is not a contamination effect of the electron beam because different regions which were not exposed to the electron beam (just the ion beam) show similar features.
- Precipitates do not amorphize as readily as 25˚C but edge is affected: morphology changes.

- Some edges (thinnest area around the holes) show material removal due to sputtering and/or atomic diffusion toward the thicker region.

4. Production of thin film sample of vapor-deposited related model alloys of desired composition and initial irradiation.

Samples were prepared, characterized and preliminary irradiations conducted in the IVEM facility.

Film deposition by the co-sputtering method: Thin film samples were created for in-situ irradiations using ion irradiation. In an evacuated chamber, an argon partial pressure of approximately 0.05mbar is established through a gas dosing valve, and a glow discharge is ignited between an anode (specimen) and a cathode (metal target) by means of high voltage. The resulting positively charged argon ions are accelerated toward the cathode and through their impingement knock out (sputter) the metal atoms and clusters off the target. Many collisions occur between the sputtered metal atoms and the gas molecules in the process chamber, resulting in strong scattering of the metal atoms. These are deposited uniformly onto the substrate in the chamber as a homogeneous thin metal film. By controlling the thickness deposited to ~ 100 nm, the resulting film is electron-transparent enough for Transmission Electron Microscopy.

Sample preparation:

The films were processed using an iron foil (99.99% purity) obtained from Alfa Aesar and an Yttria sputtering target (99.99% purity) obtained from Williams Advanced Materials. The Fe-Y-O thin films were co-sputter deposited onto NaCl substrates and onto Si wafers (for Rutherford Backscattering Spectroscopy (RBS) characterization) using the dual gun system at a base pressure of about $7x10^{-7}$ Torr at room temperature (at the Materials Research Laboratory (MRL), Penn State University). The coated NaCl substrates were cleaved into small pieces and the specimens were floated on a de-ionized water-ethanol solution onto TEM copper grids, cleaned in de-ionized water, and dried before they were used in the IVEM. The as-deposited thin films were examined with TEM. Figure 4 shows the general appearance of the as-deposited films and the associated diffraction pattern. Indexing of the diffraction pattern showed no yttria rings, and all rings were indexed as bcc-Fe.

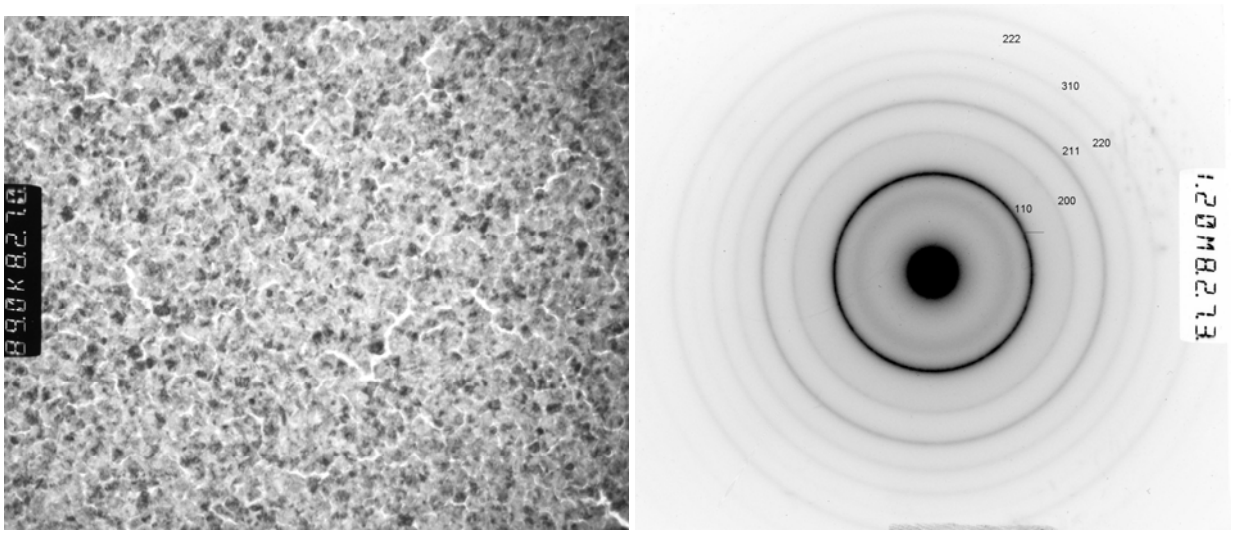

Figure 27: Transmission electron microscopy bright field micrograph (left) showing as fabricated Fe-Y-O thin film, with corresponding indexed diffraction pattern (right). Only bcc-Fe diffraction rings are observed.

Irradiation in the Intermediate Voltage Electron Microscope Facility at Argonne National Laboratory ANL

The thin films were irradiated at the IVEM-TANDEM facility at Argonne National Laboratory where an ion accelerator is attached to an electron microscope operated at 300 kV [5]. Samples can be irradiated with various ions, at a range of energies. In this case we used 500 keV Ar^{+} ions at fluxes typically around $2.50x10^{12}$ ions/cm^2-s, at room temperature. The ion-beam energy was chosen on the basis of computer simulations using SRIM-2003 [6] so that ion-implantation is minimized in the films. The total displacement damage, calculated by SRIM-2003 using a displacement energy of 25 eV, was about 80 displacements per atom (dpa) at 10^{16} ion/cm^2. Evolution of the microstructure was followed by sequentially taking images and diffraction patterns (DP) of the films while they were being irradiated and by videotape recorded on film. Individual grain sizes were obtained from direct measurement on the images. Calculations show that in the given configuration, with the sample holder in contact with the grid, itself in contact with the sample, the temperature rise in the sample was no more than 10 to 20 K. This increase is negligible in terms of irradiation induced processes.

The results of the irradiation experiment show that irradiation to 10^{16} ion/cm^2 caused Fe oxides (FeO and Fe_2O_3) to form within the film. Figure 5 shows the comparison of the initial diffraction pattern (left) and that obtained after 10^{16} ion/cm^2. The pattern at the left can be completely indexed using bcc-Fe and the one on the right shows lines that can be indexed as FeO (black arrows) and Fe_2O_3 (yellow arrows). No indications of yttrium oxide were observed, which is possibly to be expected given the low Y concentration present in the start of irradiation. Examination of the shaded region showed no change at the end of the irradiation.

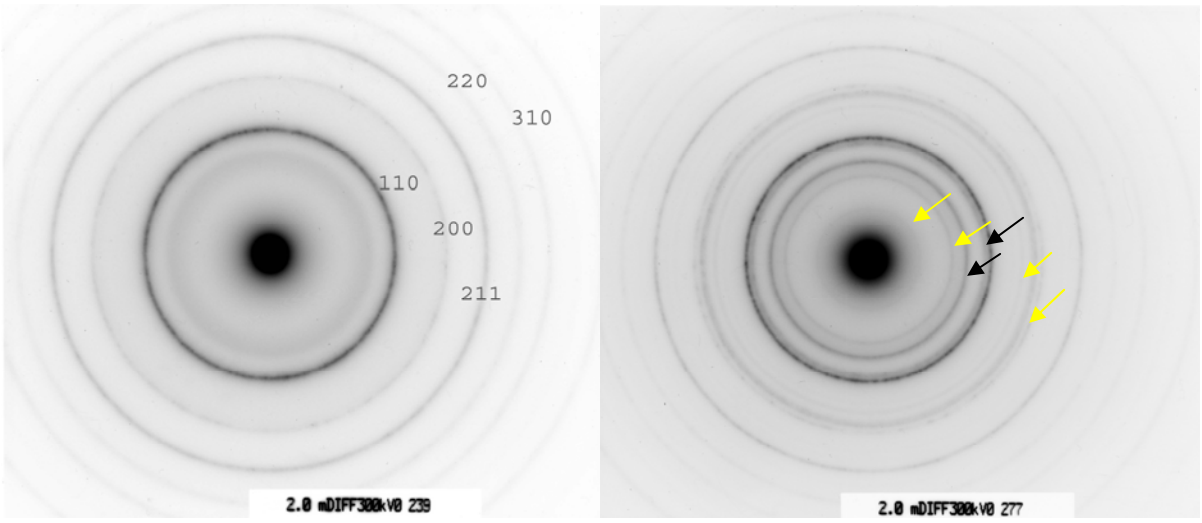

Fig 28 . Fe-Y-O sample irradiated with Ar 500 keV ions. Diffraction pattern at different fluences: prior to irradiation and after irradiation (10^{16} ions/cm^2) showing new diffraction rings characteristic of FeO (black arrows) and Fe_2O_3 (yellow), in addition to the alpha-Fe lines present throughout.

5. Conclusions:

For this study, various alloys were selected among the many MA-ODS steels available. The materials included two heats of MA-957 (from two different manufacturers), MA956, the French alloy DY, and the Japanese alloy M16 ODS steel (JNC). The materials were characterized in the as-received state using synchrotron radiation diffraction in reflection geometry, (the synchrotron radiation being capable of detecting small volume fractions of precipitates). None of the alloys exhibited diffraction peaks associated with the oxide dispersoids (yttria or titania) initially introduced, suggesting that they have been dissolved or changed their structure during processing. This highlights the fact that *thermo-mechanical treatment during the fabrication of the alloy has a critical impact on the initial dispersoid* (initially introduced as a powder). Depending on the alloys, the XRD analysis also showed the formation of intermetallic precipitates (such as the χ phase in the DY alloy) and mixed-metal carbides in the alloy containing carbon of the form $M_{23}W_2C_{12}$ (JNC alloy). In contrast, the MA957 and MA956 steels did not show carbides and intermetalics in the XRD spectra indicating that the dispersoid in these alloys is composed of oxide clusters mainly.

Also, TEM samples were processed by electro-polishing to characterize the overall grain size/morphology of the alloys as well as the precipitate morphology and size distribution. For instance, these examinations showed two populations of oxides size-wise (very fine particles (few nms) vs. larger ones (few hundreds of nms) in every alloy. The MA957 samples both from CEA and PNNL showed a lamellar grain-structure where as the JNC sample was more isotropic and had smaller grain sizes.

As a first step to understanding in-reactor behavior, irradiation with ions has been an effective means to investigate the stability of the nano-particles under irradiation. Therefore, in-situ Fe ion irradiations were conducted at the Intermediate Voltage Electron Microscope (IVEM) at Argonne National Laboratory using 300 keV Fe ions at both room temperature and 500ºC to more than $3x10^{15}$ ions/cm^2.

The Fe ion irradiations at 25ºC show degradation of particle interfaces rather early in the irradiation stage. Particle amorphization was observed at this irradiation temperature ; however it was noticed that some particles are more resistant to amorphization than others; this difference in behavior most likely comes from the difference in chemical composition. EDS characterization proves inadequate to probe particles of such sizes because the size of the beam is bigger than the particles and therefore the spectrum always includes part of the matrix. Energy filtering using a GIF appears to be a more adequate tool for such purpose. This was not possible during the timr frame of the last phase of this project.

After irradiation the small precipitates are more difficult to find. This may be because at 25ºC, irradiation damage does not anneal as fast as higher temperature hence it is more visible than at higher temperature (“black dot damage”, loops etc); this makes it more difficult to see the small size particle population even though the dose in not very high. In the neutron irradiation study [4], it was reported that the small size oxides disappeared at high doses (200 dpa). Also in the neutron irradiations, the big precipitates dissolve and are surrounded by a “halo” of small precipitates.

In the MA957, the particles seemed more resistant to amorphization than those in DY or M16 which also contain intermetallics (DY) and carbides (JNC). Most particles are still crystalline in MA957 even though some particles have an altered edge (few). It should be reminded that in the MA957 (and MA956) did not show traces of carbides or intermetallics in the XRD spectra, indicating that the dispersoid in these alloys is composed of oxide clusters mainly. *The local chemistry of the clusters impacts its stability under irradiation.* The stability of the carbides or intermetallics is expected to be different from the oxide clusters since the threshold energies for displacements of the different atomic species are different and depend on the compound formula and structure.

At 500ºC the dispersoid particles appeared to be more stable as far as amorphization, indicating that *temperature is an influential parameter in determining the stability of these particles*. Nevertheless, the particle surface morphology is altered.

Student theses generated during the project at Penn State

Djamel Kaoumi, Ph.D Thesis in Nuclear Engineering; graduation date: May 2007;
"Microstructure Evolution of Nanocrystalline Thin-Film under In-Situ Ion-Beam Irradiation."

Publications: [7-9]

Conferences: TMS, Orlando, Florida, March 2007;
MATGEN-IV Cargese, Corsica: 2 presentations:

Grain Growth in Nanocrystalline Metals under *In Situ* Ion-Beam Irradiation, D.Kaoumi, A.Motta and R.Birtcher

Characterization and in-situ Fe ion irradiation of four MA-ODS steels of interest for structural applications in GEN-IV nuclear reactors, D. Kaoumi, A.Motta and M.Kirk

References

[1] A. Alamo, "Microstructure and textures of ODS ferritic alloys obtained by mechanical alloying," Materials Science Forum, (1992), Trans Tech Publications, Switzerland, vol., 183-190.

[2] R. Klueh, D. S. Gelles, S. Jitsukawa, A. Kimura, G. R. Odette, B. van der Schaaf, and M. Victoria, "Ferritic/Martensitic Steels an overview of recent results," Journal of Nuclear Materials, vol. 307-311, (2002), 455-465.

[3] R. L. Klueh and D. R. Harries, High Chromium Ferritic and Martensitic Steels for Nuclear Applications. West Conshohocken, PA: ASTM, 2001.

[4] I. Monnet, P. Dubuisson, Y. Serruys, M. O. Ruault, O. Kaïtasov, and B. Jouffrey, "Microstructural investigation of the stability under irradiation of Oxide Dispersion Strengthened ferritic steels," Journal of Nuclear Materials, vol. 335, (2004), 311-321.

[5] C. W. Allen and E. A. Ryan, "In-Situ Ion Beam Research in Argonne's Intermediate Voltage Electron Microscope," Mat.Res. Soc. Simp. Proc., (1997), vol. 439, 277-288.

[6] J. Ziegler, J. P. Biersack, and U. Littmark, The Stopping and Range of Ions in Matter. New York: Pergamon Press, 1985.

[7] D. Kaoumi, A. T. Motta, and R. C. Birtcher, "Grain Growth in Nanocrystalline Metal Thin Films under In Situ Ion-Beam Irradiation," Journal of ASTM International, vol. submitted, (2006).

[8] D. Kaoumi, A. T. Motta, and R. C. Birtcher, "Irradiation-Enhanced Second-Phase Precipitation in Zr-Fe Nanocrystalline Thin Films," MRS Symposium Proceedings, Boston, MA, (2005), vol. Vol. 908E.

[9] D. Kaoumi, A. Motta, and R. C. Birtcher, "Grain growth in Zr-Fe thin films during in situ ion irradiation in a TEM," Nuclear Instruments and Methods in Physics Research B, vol. 242, (2005), 490-493.